FIRST SPIRE: Optical Error Budgets

RAL	K.King			
	B.Swinyard	**X**		
CNES	M.Joubert		Y.Blanc	
CEA-Sap	Jean-Louis Auguères			
LAS	J.P.Baluteau	**X**	D. Ferrand	
	K.Dohlen	**X**	R. Malina	
	A.Origné	**X**	P.Dargent	**X**
	D.Pouliquen	**X**		

LABORATOIRE D'**A**STRONOMIE **S**PATIALE - CNRS BP 8 13376 MARSEILLE Cedex 12 FRANCE

Tél : (33) +4 91 05 59 00 - Fax : (33) +4 91 05 69 59

Updates

Date	Indice	Remarks
22 May 2000	1	Creation of the document

Reference documents

#	Title	Author(s)	Reference	Date

Host system	Windows NT
Word processor	Microsoft Word 97
File	LOOM.KD.SPIRE.2000.002_Optical_Error_Budgets.DOC

1. Scope

2. Introduction

Preliminary optical error budgets for the SPIRE instruments are presented. Throughput and wavefront error (Strehl ratio) budgets are presented for both photometer and spectrometer channels. Alignment tolerances are considered by way of a pupil alignment budget for the photometer and an interferogram contrast budget for the spectrometer.

2.1. Baseline designs

Current baselines are BOLPHT153 for the photometer channel and BOLSP501 for the spectrometer channel. The systems are shown in Figure 1.

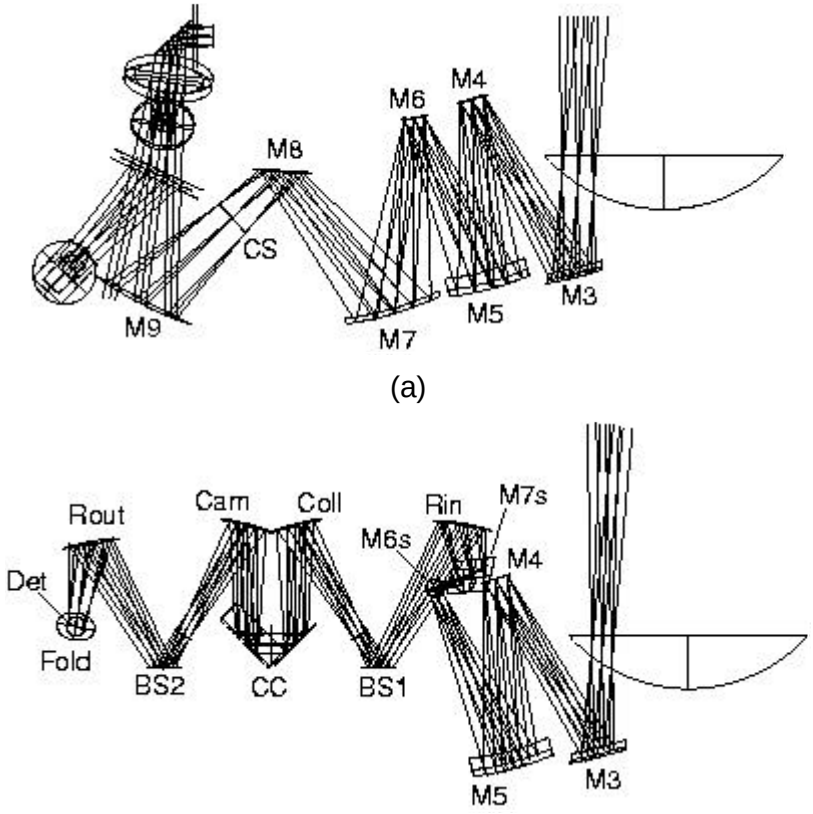

Figure 1. Ray diagram of the photometer channel (a) and spectrometer channel (b) of the SPIRE instrument showing the ray paths for three points in the tangential plane, centre and extremes of the FOV (±2′). The symmetrical lower half of the spectrometer channel is generated by reflection about the plane containing the two beam splitters.

3. Photometer budgets

3.1. Throughput

Apart from filters and dichroics, major part of budget is due to sizing of cold stop. Undersizing has been assumed, but stray light modelling indicates that this may not be required, in which case this part will be improved. Loss due to cold stop size is estimated geometrically according to the relative pupil alignment parameter $\Delta R/R$ as defined in Sec. 3.3. Three options exist:

1) Undersizing: no detector is allowed to see outside the telescope pupil (M2) ($T = 1 - 2\,\Delta R/R$),

2) Exact sizing: On average, the detectors see the entire telescope pupil, but some detectors may see a little more (ie surrounds), others a little less ($T = 1 - \Delta R/R$),

3)Oversizing: All detectors see the entire telescope pupil (and in general some of its surrounds) ($T = 1$).

The reason for choosing undersizing is to limit background radiation from M2 surrounds and their variation, especially during chopping.

Diffraction and baffling losses have still to be precisely calculated.

Optics losses assume a reflectivity per surface of 99%.

Current throughput budget is below the IRD requirement. A change in cold-stop sizing philosophy would improve the situation.

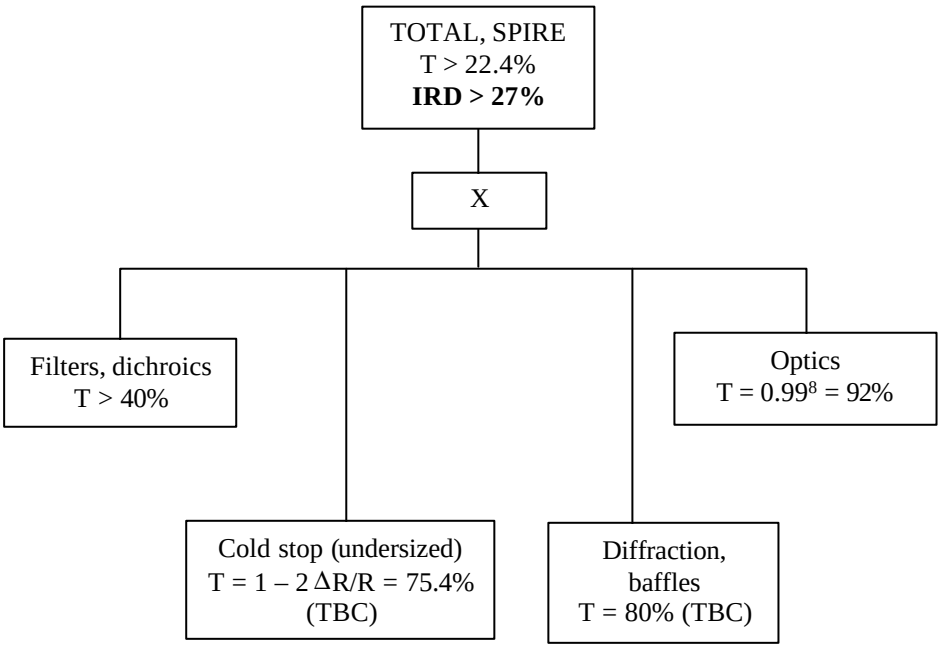

Figure 1. Photometer throughput budget.

3.2. Wavefront error

RMS wavefront errors (WFErms) are calculated at 250 µm. Total budget is obtained by RSS summing of individual budget values. Strehl ratio is calculated by the Marechal approximation:

$$S \approx 1 - 4p^2\, WFErms^2 = 1 - 4p^2 \sum_i WFErms_i^2$$

The budget is well within the requirement. Note particularly that alignment errors as described in Sec. 3.3 contribute very little to the budget. The margin may be used to relax surface shape and/or focus requirements, but neither of these seem to be overly hard to reach.

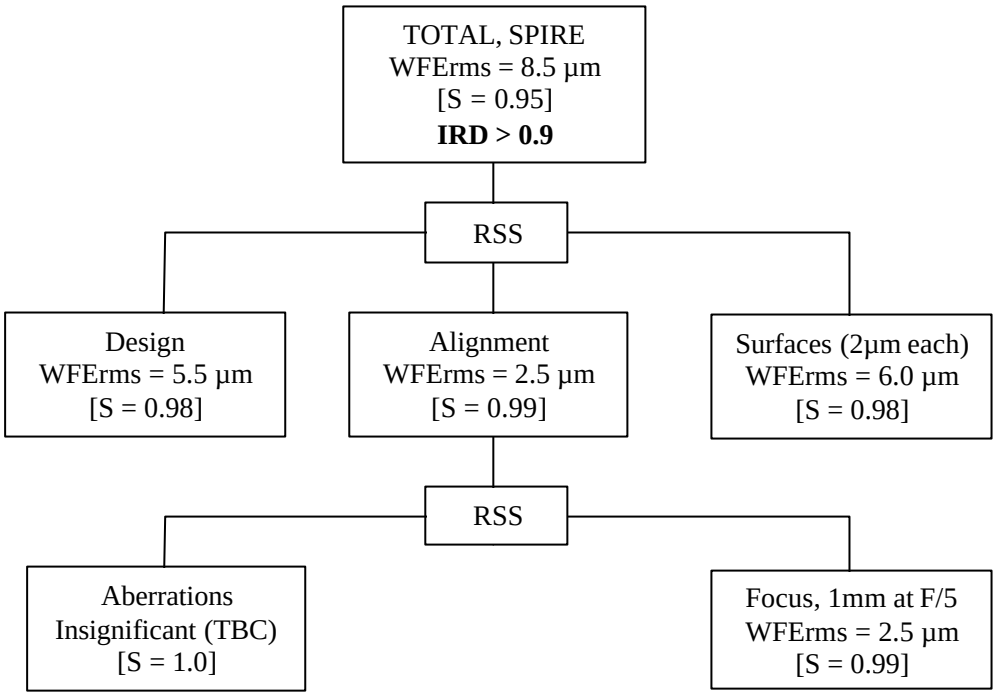

Figure 2

3.3. Pupil alignment

The pupil amignment budget is dimensioning for mechanical tolerances in the photometer case. There is no IRD on pupil alignment, but, as has been shown in the above throughput budget, it has a strong influence on instrument throughput.

The three major components concern design and alignment (FIRST and SPIRE), outlined in heavy lines in the figure. The design value quantifies the variation in pupil position for different points in the FOV for a perfectly aligned instrument. It is due to pupil aberrations. We believe that this value has been minimized for the optical concept chosen, and that a further reduction would require important complications of the optical design.

Degradation of pupil alignment due to mechanical misalignment consists of errors under ESA control (alignment between the FIRST telescope and its instrument interface bench, referred to here as the F-bench) and errors under SPIRE control. The latter is again broken down to errors due to the FIRST - SPIRE interface (F-bench to S-bench), interfaces between SPIRE structure and mirrors, and interface between SPIRE structure and the cold-stop itself.

Apart from an uncertainty in the actual ESA alignment specification (due to a lack of information in the ESA alignment document), the budget shows a good balance between its three major components. The contribution from instrument alignment is the smallest, indicating that no great improvement can be expected from reducing the mechanical tolerance values.

Mechanical tolerances have been set to 0.1mm decenter for each component along each direction x, y, z and 1arcmin tilt for each component around each axis. The effect of misalignments equal to these values for each component and axis are obtained from a sensitivity analysis, summarized in Figure 4 (BolPhtRev05.mac, SpirePhotTol18.xls). Verification of the effect of random distributions of alignment errors is shown by the histogram plot of Figure 5 (SpirePhotTol20.xls).

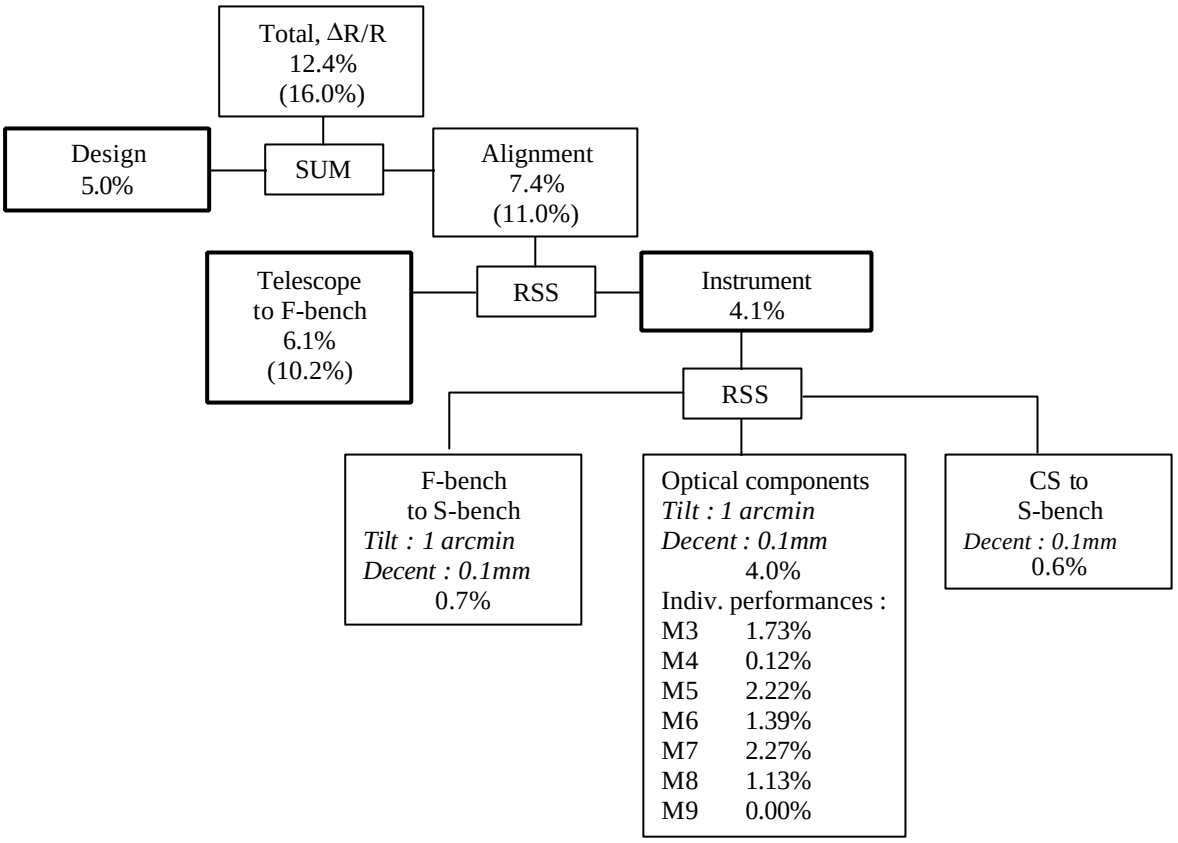

Figure 3. Pupil alignment budget for the photometer. The heavy boxes indicate the tree major components of the budget: optical design (pupil aberrations) telescope alignment under ESA responsibility, and SPIRE alignment. Numbers in brackets indicate an uncertainty in the ESA alignment budget.

The SPIRE alignment budget assumes mounting accuracy of 0.1mm and 1arcmin for each interface: the SPIRE bench (S-bench) mounted on the FIRST bench (F-bench), each mirror in the optical train mounted on the S-bench, and the cold stop (CS) mounted on the S-bench. These tolerances should in each case be distributed on the required intermediate interfaces. For example, the CS is mounted on the 2K box which is in turn mounted on the S-bench.

The two top budget components, design and alignment, are summed because the pupil aberrations are deterministic. All other components are "root-sum-squared". As shown by Monte-Carlo simulation (Figure 5 below), assuming a uniform statistical distribution of errors within the tolerance bounds, this budget covers more than 90% percent of the real cases.

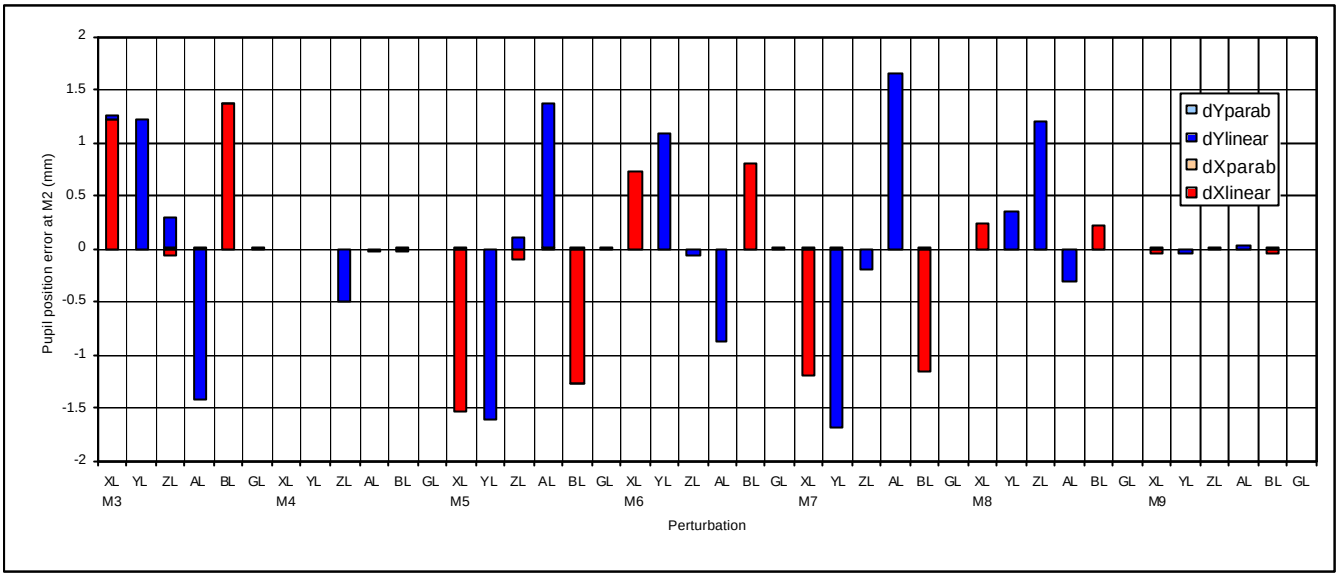

Figure 4. Sensitivity of each photometer mirror to 0.1mm decenter tolerance (XL along x axis, YL along y axis, ZL along z axis) and to 1arcmin rotation tolerance (AL around x axis, BL around y axis, GL around z axis). Apart from M3 and M5, the z axis is perpendicular to each surface at its apex, the y axis is perpendicular to z in the plane of the system, the x axis is perpendicular to y and z. For M3 and M5, the z axis is shifted by 20mm so as to coincide approximately with the centre of gravity of the mirrors, and tilted so as to be perpendicular to the surface at that point.

Results are in mm measured at the M2. For an M2 radius of 150mm, an error DR = 1mm corresponds to a fractional pupil alignment error of DR/R = 0.67%. Red bars show displacements along the x direction, blue bars along the y direction. Light blue and light red correspond to non-linear sensitivity components: these are clearly insignificant.

Apart from M4 (conjugated with the pupil) and M9 (not involved in pupil imaging since after the cold stop), all mirrors have similar sensitivities. Errors due to GL tilts (azimuth rotation) are very small for all mirrors, the alignment budget is not dimensioning for these perturbations. A tolerance of about 0.5 degrees is probably acceptable to avoid vignetting.

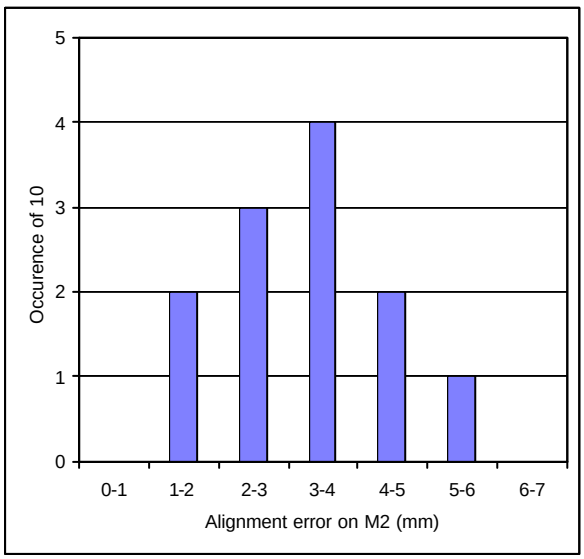

Figure 5. Monte Carlo analysis with 10 randomly generated combinations of alignment errors. Each mirror has been given decenters and tilts up to ±0.1mm and ±1arcmin in each direction with an even satistical distribution. The resulting average error is 3.4mm (DR/R = 2.2%) and the 90% percentile is at 4.8mm (DR/R = 3.2%), i.e. less than the RSS assumption made in the error budget (Figure 3). This provides a "confidence margin". [The RSS assumption actually works with standard deviations. Since the standard deviation of an even distribution between ±a is s = a/Ö3, there is a factor Ö3 between the Monte-Carlo average and the RSS sum: 2.2% Ö3 = 3.8%, compared with 4.0% in the budget.]

4. Spectrometer budgets

4.1. Throughput

In the spectrometer case, the elimination of flux from M2 surrounds has been judged less of a problem, particularly because the spectrometer does not rely on chopping (signal is modulated by the FTS itself). We have therefore assumed an oversized (no-loss) cold stop. Assuming 20% loss due to diffraction and baffling and taking account of the maximum theoretical throughput of 50% due to band-pass filtering of each output, the total budget predicts a total throughput of 14% instead of the required 20%.

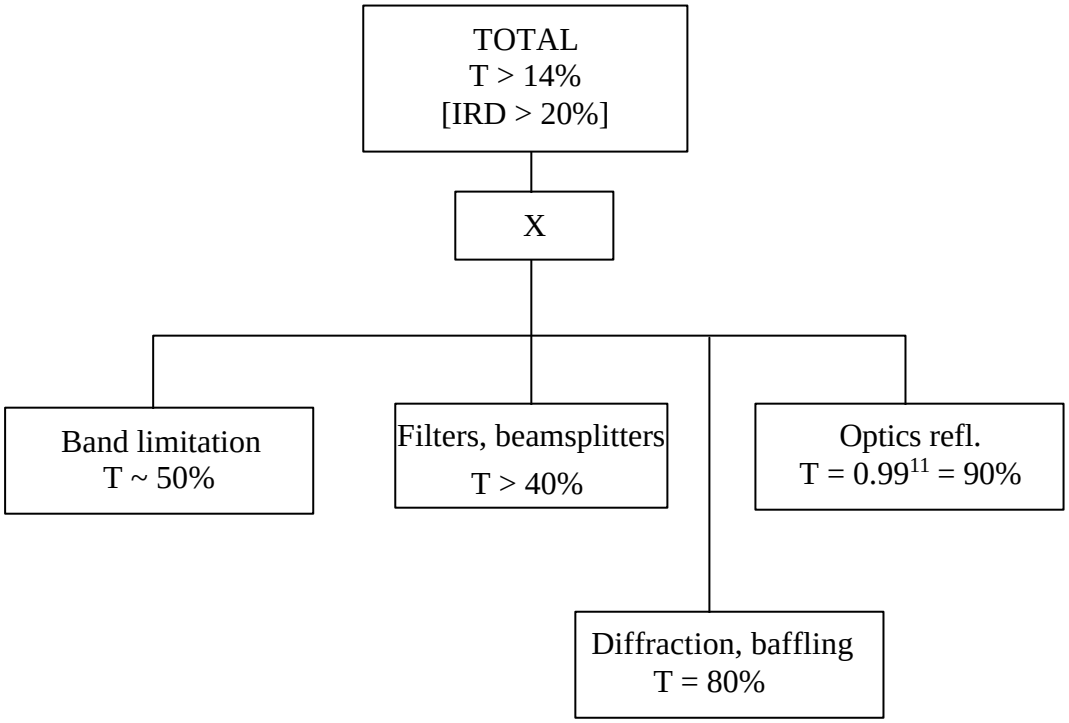

Figure 6. Spectrometer throughput budget.

4.2. Wavefront error

Wavefront error budget meets IRD with margin. See Sec. 3.2 for comments.

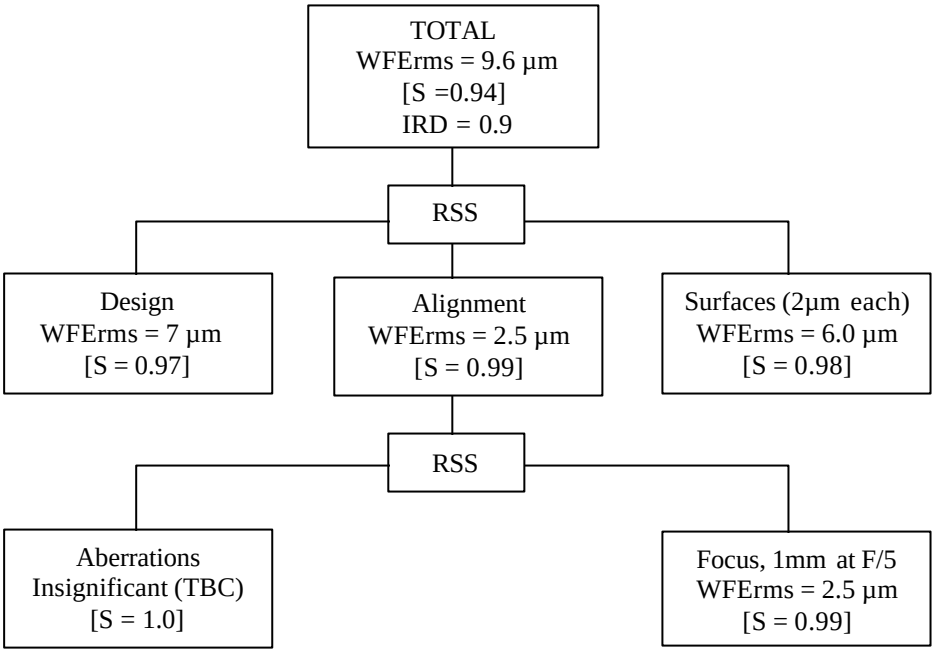

Figure 7. Spectrometer wavefront budget.

4.3. Interferogram contrast

Interferogram contrast describes the efficiency with which the instrument renders the undulating interference intensity created by the FTS. It is defined for a monochromatic beam as:

$$k = \frac{I_{max} - I_{min}}{I_{max} + I_{min}} \quad (1)$$

where I_{max} and I_{min} are maximum and minimum intensities, respectively.

Contrast is affected by tilt and shear between the interfering wavefronts. When OPD > 0, wavefronts from an off-axis object are sheared due to geometry, and may be tilted due to differential distortion. Misalignments of components within the interferometer also introduce tilt and shear.

When interfering wavefronts are tilted by angle θ, the image on the detector is shifted by a displacement $\Delta = \theta f$ where f is the camera focal length. Using the van Cittert Zernike theorem, Lambert and Richards (1978) calculate the resulting fringe contrast as:

$$k_T = 2J_1(u)/u \quad (2)$$

where $u = 2\pi\Delta/(\lambda F)$. Eq. (2) assumes an evenly illuminated aperture stop, it is therefore a conservative approximation for SPIRE since the Gaussian-mode beam tends to underilluminate the pupil, hence increase F and decrease u. The actual contrast loss is therefore less than estimated from the above formula.

Applying Taylor expansion to eq. (2) provides an approximation valid for small perturbations:

$$k_T \approx 1 - u^2/8 = 1 - 0.79\Delta^2 \quad (3)$$

when λ = 250µm and F = 5.

When wavefronts are sheared, the two interfering beams enter the focal plane at different angles, hence creating fringes across each detector. The detector integrates the fringe intensity hence reduces apparent fringe contrast. It is easy to see that for a square detector with uniform response the contrast becomes zero when the fringe period is equal to the detector width. The contrast is in this case described by a sinc function and may be expressed as:

$$k_S = \sin(u)/u \quad (4)$$

where u = πws/(Fλd), w is detector width, s is pupil shear, and d is pupil diameter. Assuming w = 2Fλ, the argument simplifies to: u = 2πs/d. Again this is a conservative approximation of the actual case of horn detectors with Gaussian response and circular aperture.

Applying Taylor expansion to this formula gives:

$$k_S \approx 1 - u^2/6 = 1 - 0.011 s^2 \quad (5)$$

when d = 25mm.

4.3.1. Optical design

Two sources of contrast loss due to optical design are identified:

1) Shear for off-axis object. An off-axis beam travelling through the interferometer at angle β has a shear of

$$s = OPD \sin\beta \approx OPD\ \beta$$

The angle β for an object at the edge of the FOV is given by the Lagrange invariant as

$$\beta = FOV\ D/(2d)$$

where FOV is diameter of the sky field of view and D is the telescope entrance pupil diameter. Assuming FOV = 2.6′, D = 3300mm, d = 25mm, we get β = 2.86°. At the nominal resolving power of 100, the maximum OPD is 12.5mm, hence pupil shear is s = 0.62mm. At maximum resolving power (1000), the shear is s = 6.2mm. Contrasts estimated by eq (5) are 99.6% and 64%, respectively.

2) Tilt due to differential distortion. Since there is powered optics within the interferometer and the OPD scanning causes a longitudinal displacement of the exit pupil, differential aberrations between the two interfering beams may occur. No significant difference in wavefront error has been detected, but a slight difference in distortion causes a shift of the image position (ie wavefront tilt) for off-axis objects. The shift increases linearly with OPD and reaches Δ = 0.04mm at R = 100 and Δ = 0.4mm at R = 1000. Contrasts estimated by eq. (3) are 99.8% and 88%, respectively.

4.3.2. Interferometer alignment

Contrary to optical design losses, alignment losses are independent of OPD and FOV. Tilts and decenters of each component within the interferomater in general introduce both tilts and shears to the interfering wavefronts. Table 1 gives wavefront tilts and shears produced by 0.1mm decenters and 1′ tilts of each component within the interferometer. The RSS of tilt and decenter values are calculated, and the total budgets estimated by multiplication with $\sqrt{2}\sqrt{N}$, where the $\sqrt{2}$ factor accounts for errors in both x and y directions, and N is the number of components in each case. The total budgets shows fringe contrast in brackets.

Clearly, the most critical components are the collimator and camera mirrors. Any significant reduction in alignment precision of these components will have important impacts on the alignment budget. Beamsplitter and corner cube alignments are far less critical. Tolerances may be relaxed in these cases, this may be particularly interesting for the internal alignment of the corner cubes.

In discussions with Guy Michel and Don Jennings, it became clear that they considered some adjustment capability highly desirable, at least for the qualification model, to allow optimizing cold IR operation CIRS was originally designed without adjustments, but this was included later and proved useful during “debugging” of the qualification model. It is not clear how this could be realised in SPIRE, but it should be discussed. Don also suggests that the imaging capability of SPIRE may be utilised in the cold alignment check, eliminating the need for "cold fiddeling". TBT (=To be thought about :)

Figure 8 shows the interferometer alignment budget. Nominal (R = 100) contrast values are shown and R = 1000 values are indicated in brackets. With a total budget of 90%, the required contrast (80%) is achieved with good margin.

Table 1. Wavefront tilts and shears due to 1′ tilts and 0.1mm decenters

	1° tilt		0.1mm decenter		Total per comp, per dimension		Components	Total budgets (contrast)	
Component	**Tilt, Δ (mm)**	**Shear, σ (mm)**	**Tilt, Δ (mm)**	**Shear, σ (mm)**	**Tilt, Δ (mm)**	**Shear, σ (mm)**		**Tilt, Δ (mm)**	**Shear, σ (mm)**
Beamsplitter	0.023	0.087	0	0	0.023	0.087	2	0.046 (99.8%)	0.174 (99.97%)
Collimator	0.075	0.087	0.1	0.12	0.13	0.15	2	0.26 (95%)	0.30 (99.9%)
Camera	0.075	0.087	0.1	0.12	0.13	0.15	2	0.26 (95%)	0.30 (99.9%)
Corner cube	0	0	0	0.2	0	0.2	2	0 (100%)	0.40 (99.8%)
CC internal*	0.038	0	NA	NA	0.38	0	2	0.076 (99.5%)	0 (100%)
Scan axis	0	0	0	0	0	0	1	0 (100%)	0 (100%)
Total								**89.6%**	

*) Misaligned CC facets cause 1′ beam deviation between input and output beams.

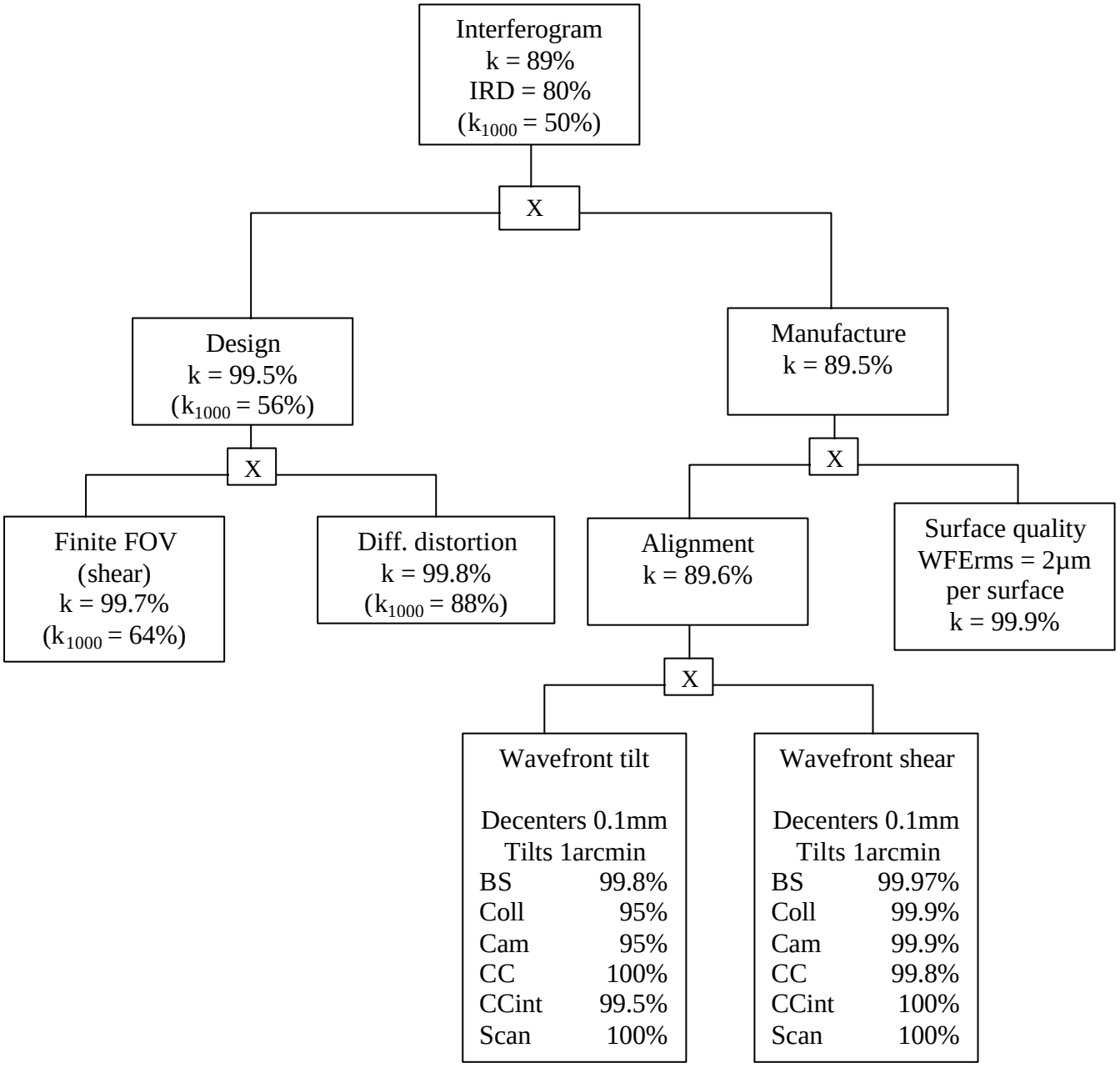

Figure 8. Interferometer alignment budget. Nominal (R = 100) contrast values are shown and R = 1000 values are indicated in brackets. With a total budget of 90%, the required contrast (80%) is achieved with good margin.